CHEMISTRY
A EUROPEAN JOURNAL

Supporting Information

© Copyright Wiley-VCH Verlag GmbH & Co. KGaA, 69451 Weinheim, 2012

Relative and Absolute Configuration of Vatiparol (1mg): A Novel Anti-inflammatory Polyphenol

Hui Ming Ge,[a] Han Sun,[b] Nan Jiang,[c] Yan Hua Qin,[a] Huan Dou,[a] Tong Yan,[a] Ya Yi Hou,[a] Christian Griesinger,*[b] and Ren Xiang Tan*[a]

chem_201104078_sm_miscellaneous_information.pdf

Relative and absolute configuration of vatiparol (1 mg), a novel anti-inflammatory polyphenol

Hui Ming Ge,[†[a]] Han Sun,[†[b]] Nan Jiang,[[c]] Yan Hua Qin,[[a]] Huan Dou,[[a]] Tong Yan,[[a]] Ya Yi Hou,[[a]] Christian Griesinger,*[[b]] and Ren Xiang Tan*[[a]]

[a] Institute of Functional Biomolecules, State Key Laboratory of Pharmaceutical Biotechnology, Nanjing University, Nanjing, 210093, China; [b] Department of NMR-Based Structural Biology, Max Planck Institute for Biophysical Chemistry, Am Fassberg 11, Göttingen 37077, Germany); [c] School of Pharmacy, Nanjing Medical University, Nanjing 210029 China

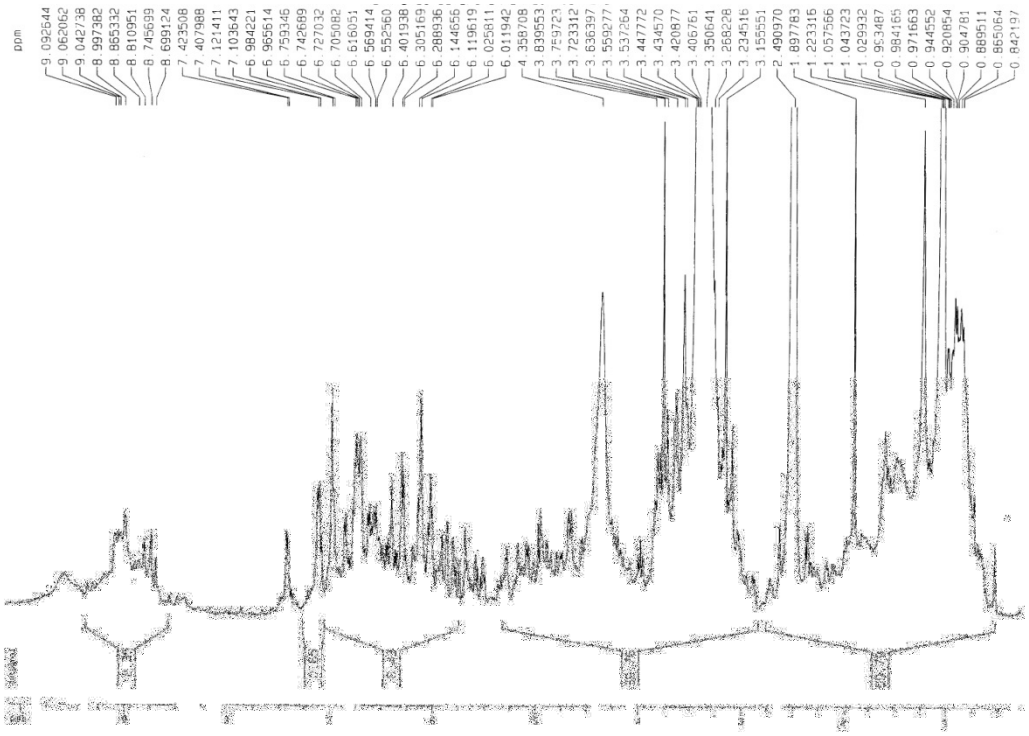

Figure S1. ^{1}H NMR spectrum of crude extract of *Vatica parviforia* (DMSO-d_6)

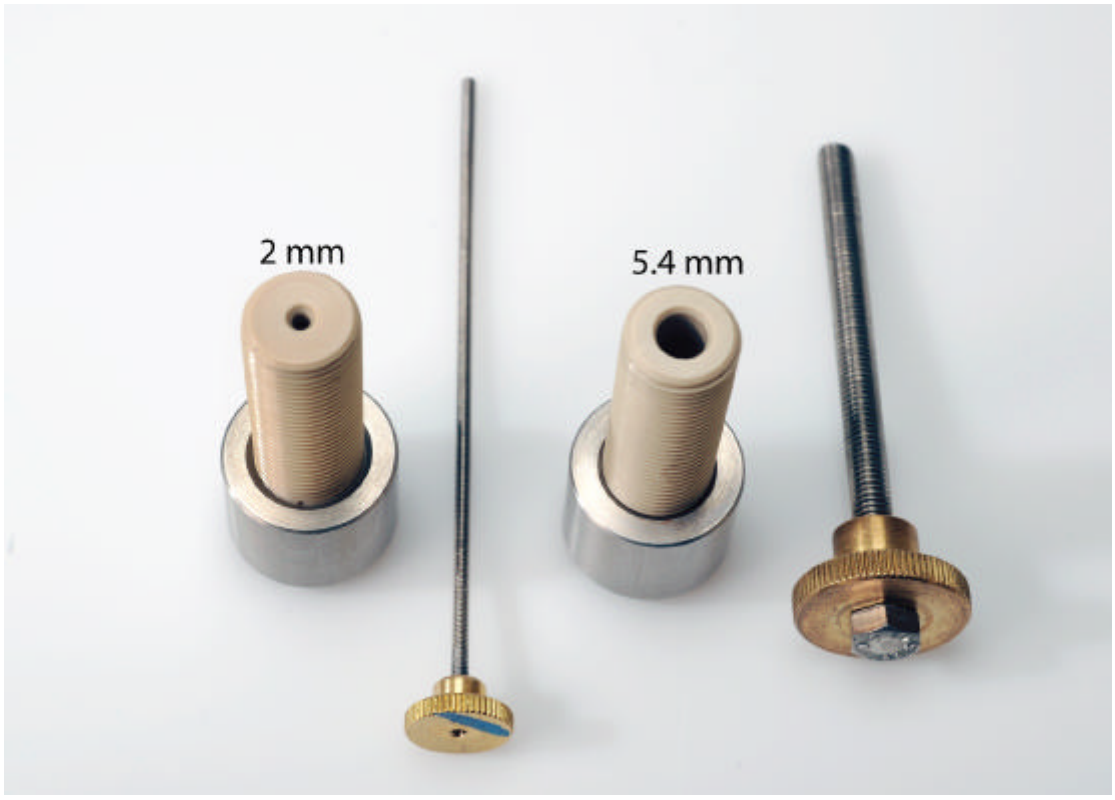

Figure S2. Comparison of the Gel cylinders with two different outer diameters (2 mm and 5.4 mm) for preparing the PH-gels in different size of NMR tubes (1.7 mm and 5 mm).

Determination of the relative configuration using RDC-enhanced NMR spectroscopy

NMR measurement of vatiparol in DMSO-d_6.

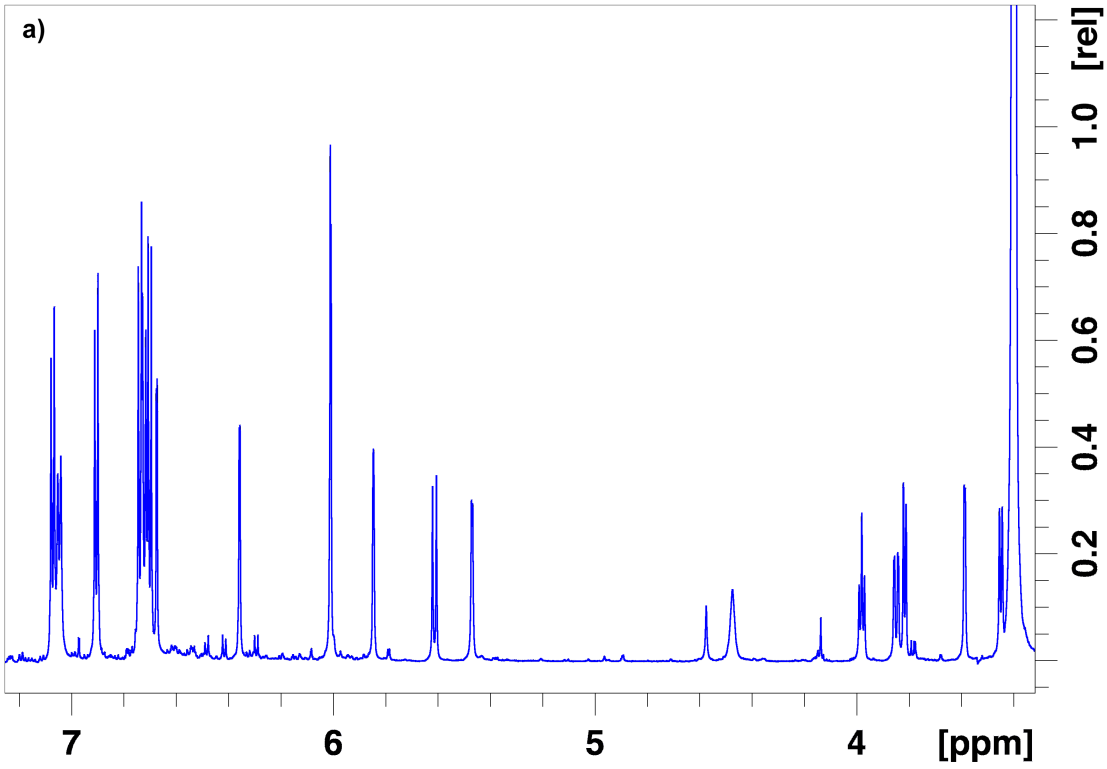

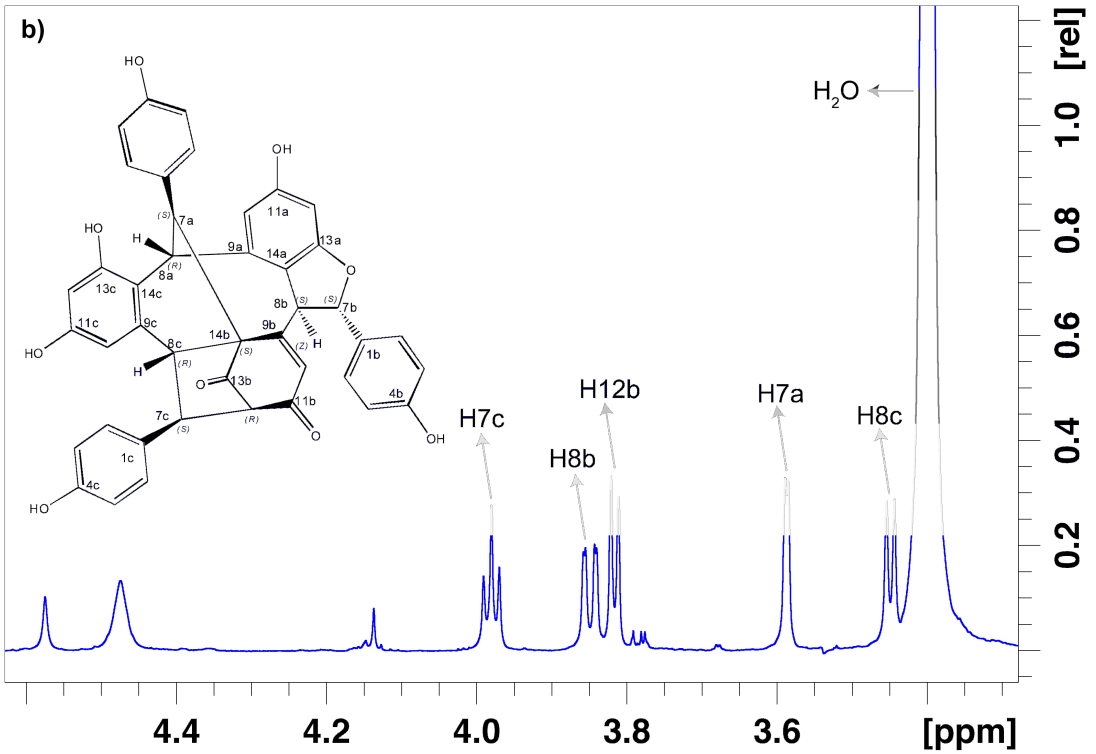

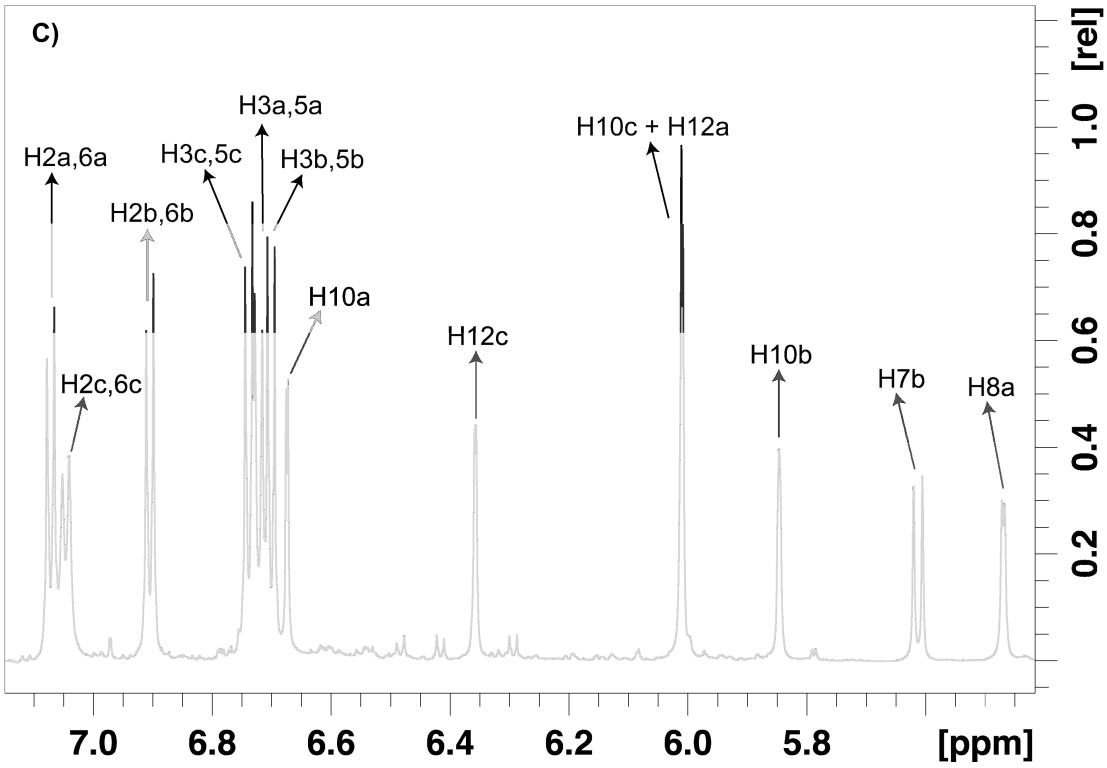

Figure S3. The ^{1}H NMR spectrum of vatiparol at 700 MHz. a) Full spectrum, b) 3.3-4.6 ppm, and c) 5.4-7.1 ppm.

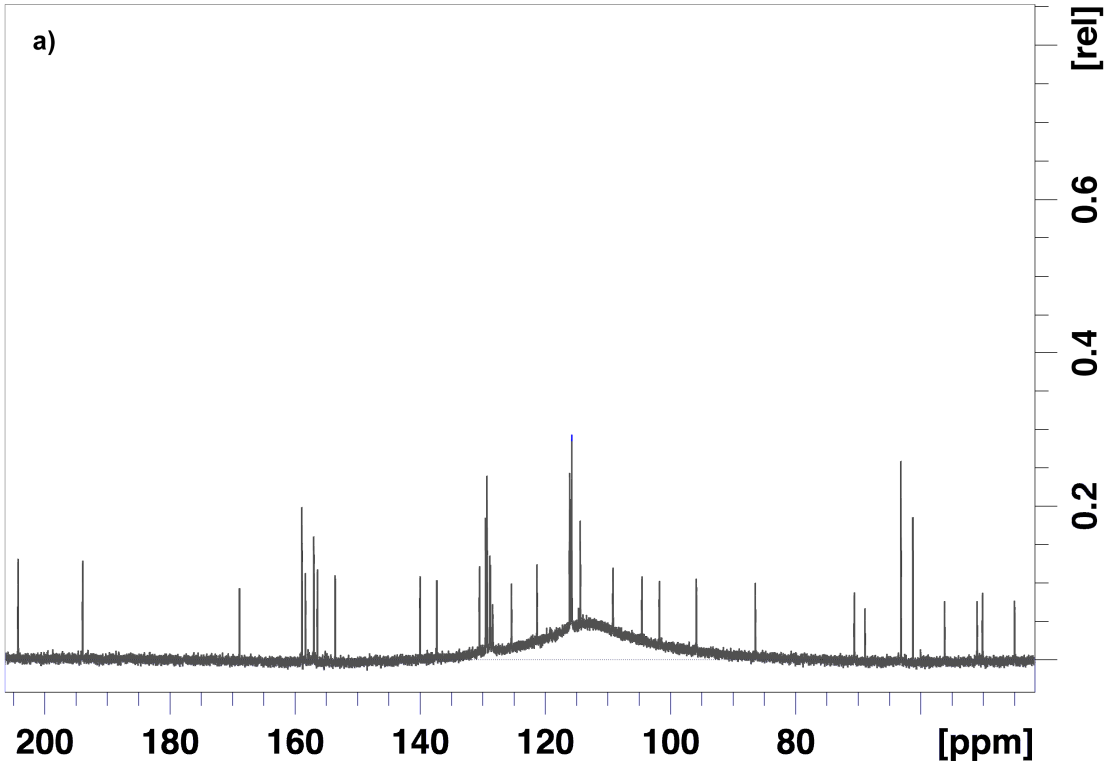

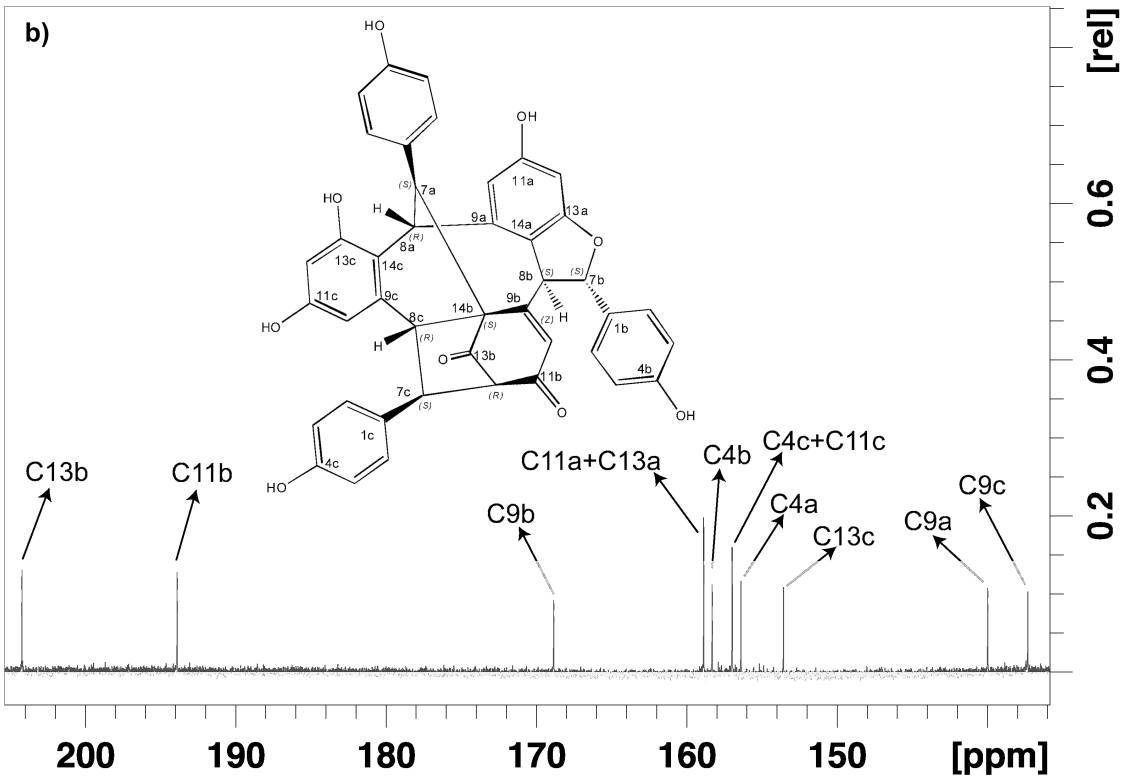
b)
HO
OH
11a
13a
9a
14a
O
7a
(S)
H
(R)
8a
13c
14c
HO
11c
9c
8c
14b
9b
8b
(S)
(S)
7b
(S)
(Z)
H
1b
HO
H
(R)
(S)
O
13b
11b
4b
OH
7c
(S)
(R)
O
1c
4c
HO
C13b
C11b
C11a+C13a
C4b
C4c+C11c
C9c
C9b
C4a
C13c
C9a
0.2
0.4
0.6
[rel]
200
190
180
170
160
150
[ppm]

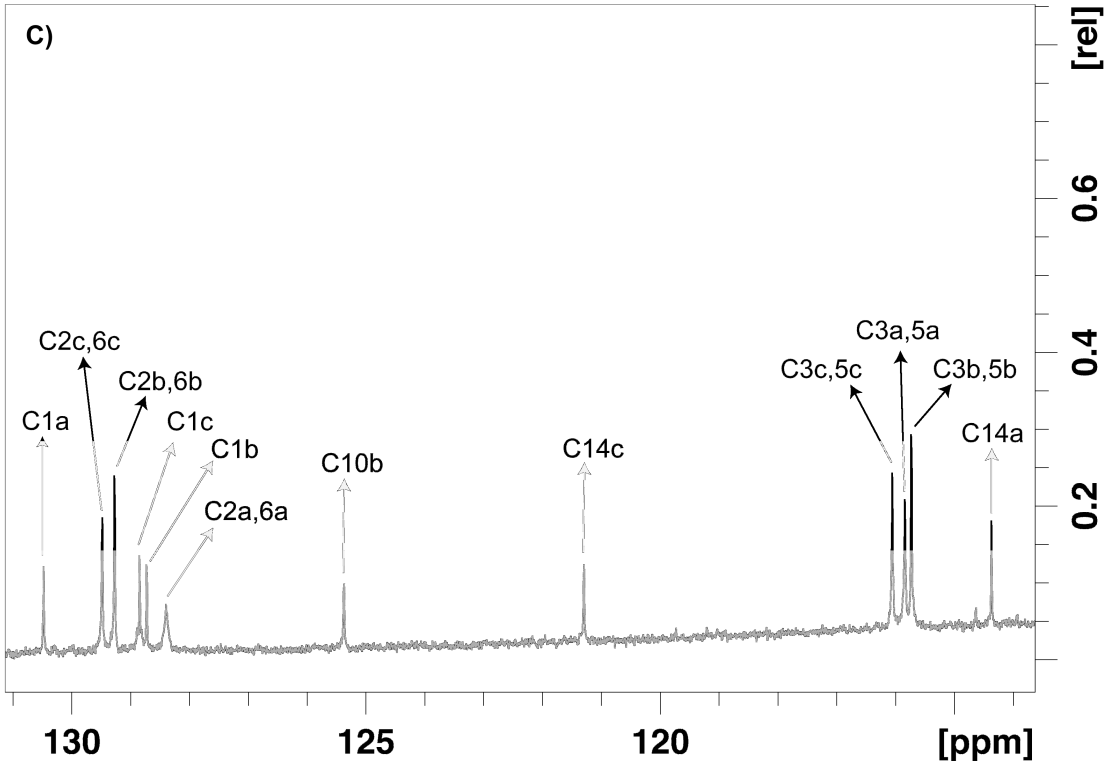
C)
C2c,6c
C2b,6b
C1a
C1c
C1b
C10b
C2a,6a
C14c
C3a,5a
C3c,5c
C3b,5b
C14a
0.2
0.4
0.6
[rel]
130
125
120
[ppm]

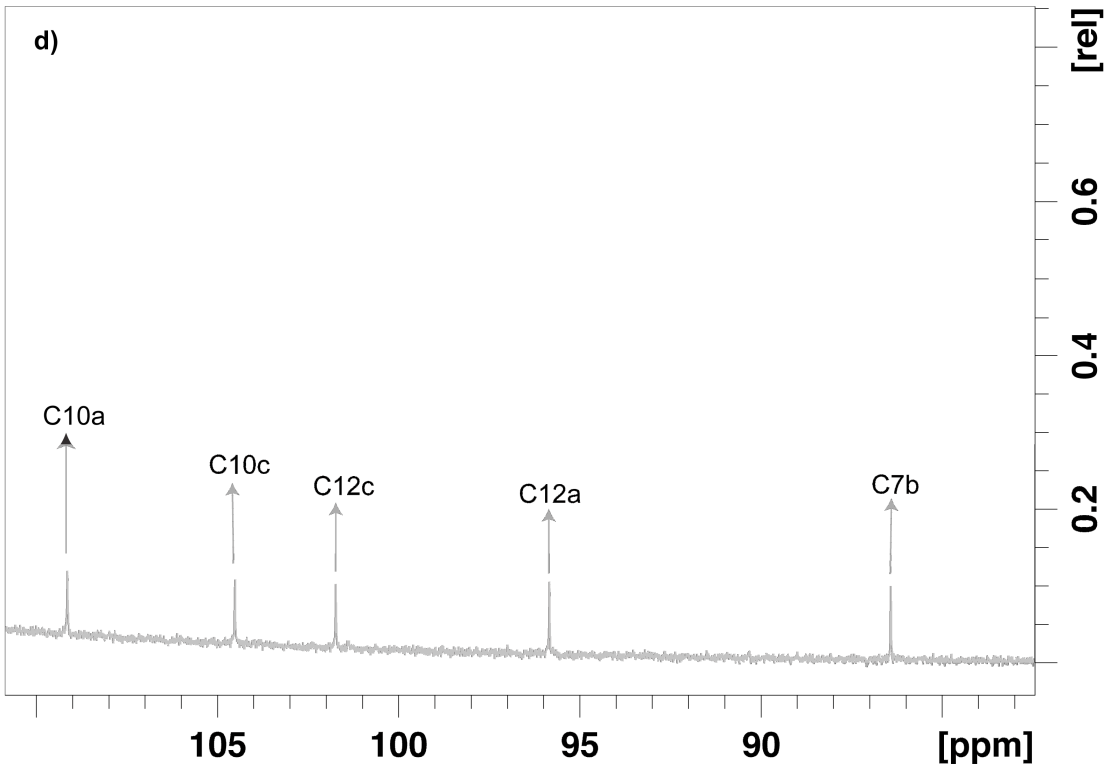

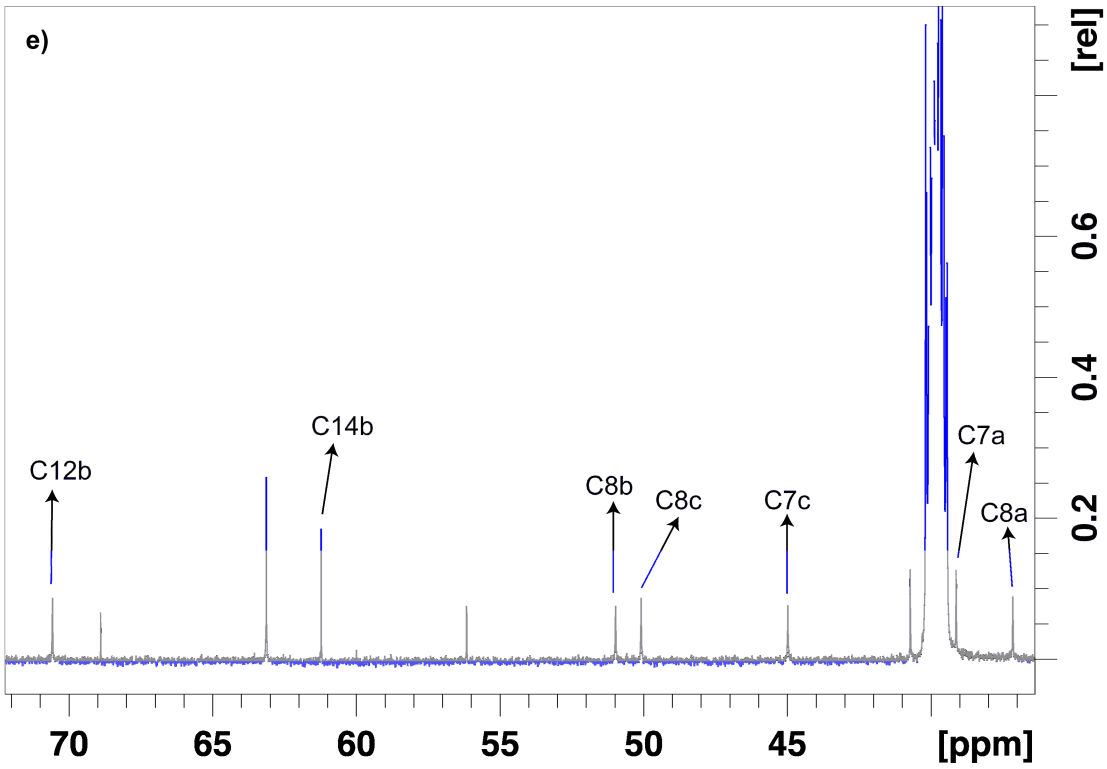

Figure S4. The ^{13}C NMR spectrum of vatiparol at 175 MHz. a) Full spectrum, b) 136-205 ppm, c) 109-131 ppm, d) 83-110 ppm, and e) 36-72 ppm.

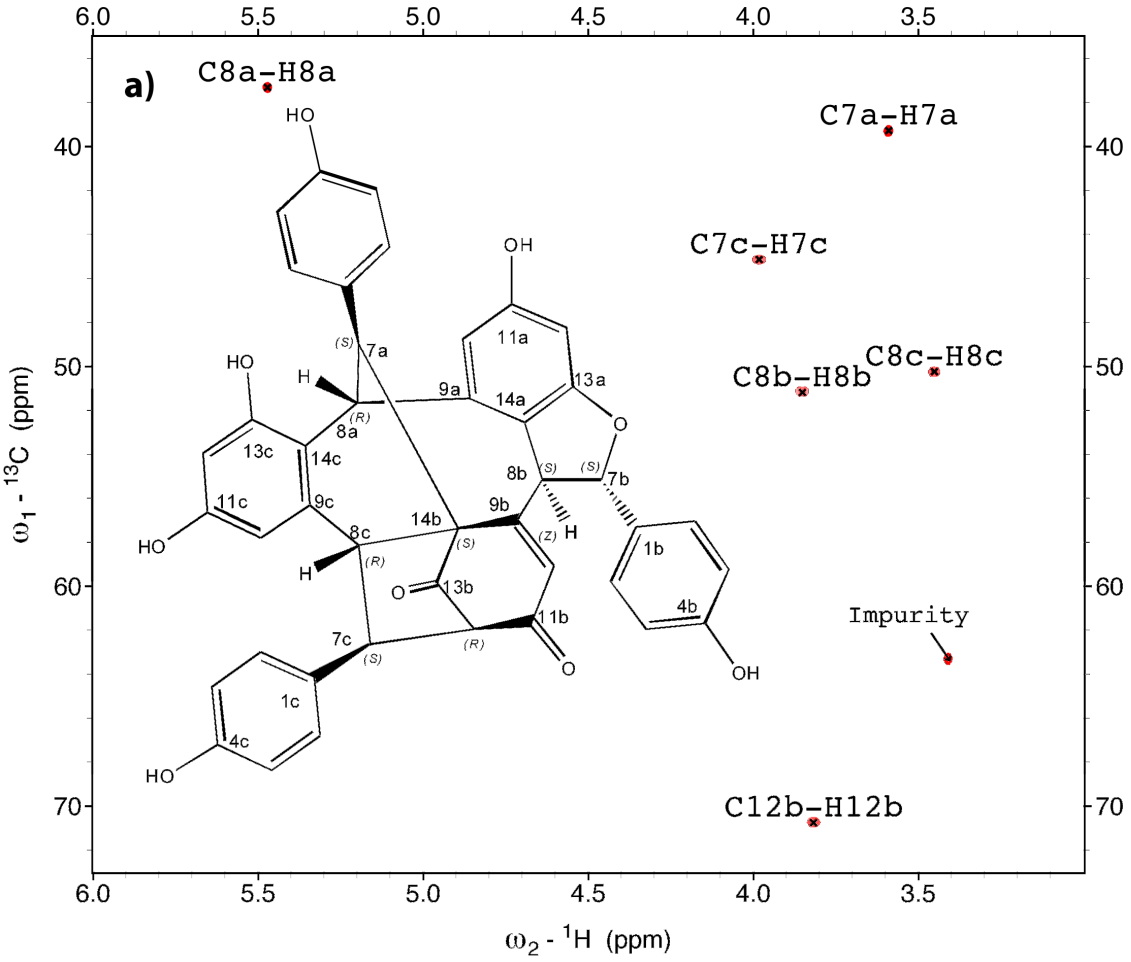
a)
C8a-H8a
C7a-H7a
C7c-H7c
C8b-H8b
C8c-H8c
Impurity
C12b-H12b
HO
OH
O
H
(S)
(R)
(Z)
7a
8a
9a
11a
13a
14a
13c
14c
11c
9c
8c
14b
9b
8b
7b
1b
4b
13b
11b
7c
1c
4c
6.0
5.5
5.0
4.5
4.0
3.5
40
50
60
70
ω1 - 13C (ppm)
ω2 - 1H (ppm)

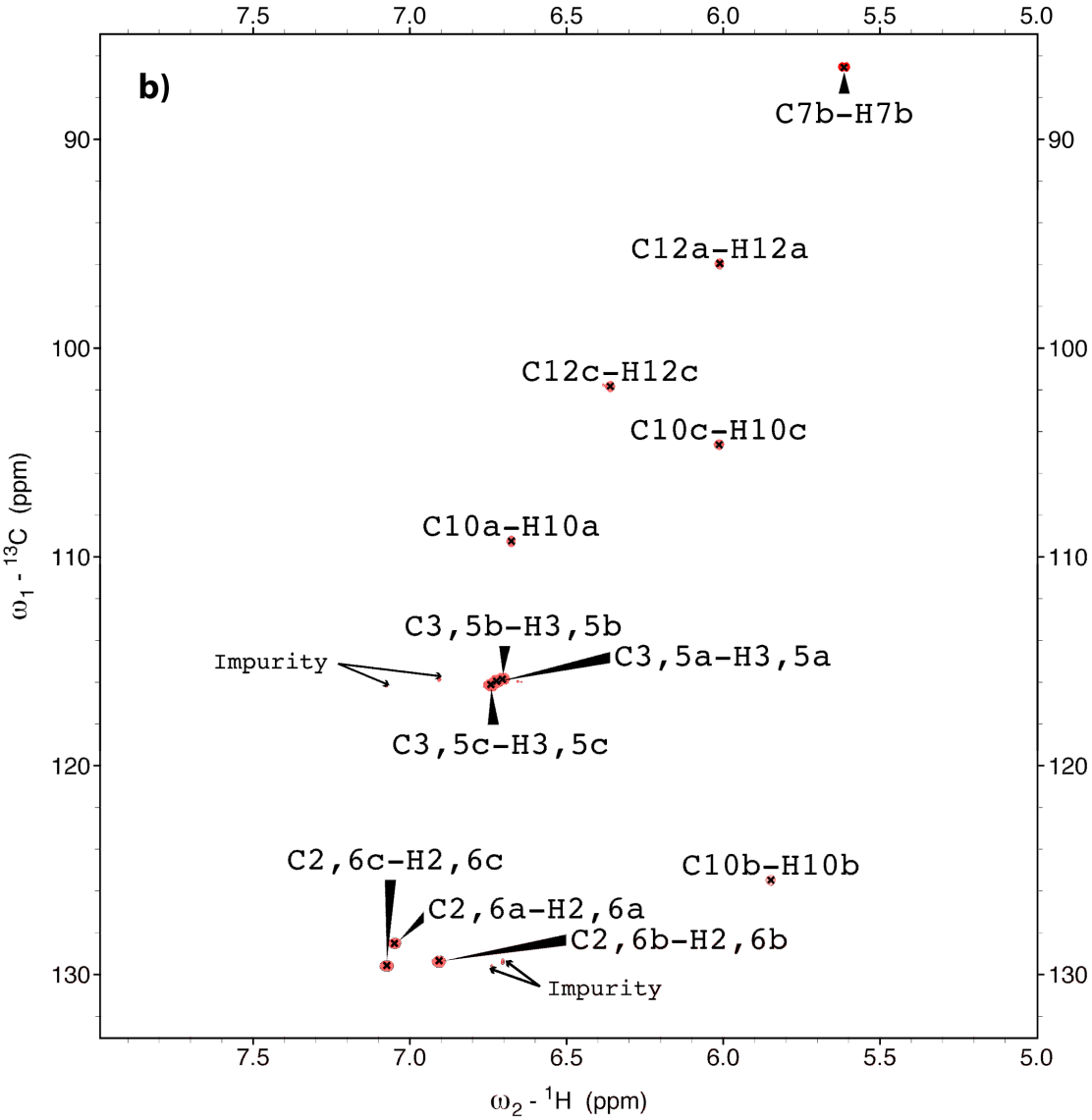

Figure S5. Two expansions of the standard ^{1}H,^{13}C-HSQC spectrum of vatiparol. a) 3.4-6.0 ppm (^{1}H) and 35-73 ppm (^{13}C) expansion, and b) 5.0-8.1 ppm (^{1}H) and 85-133 ppm (^{13}C).

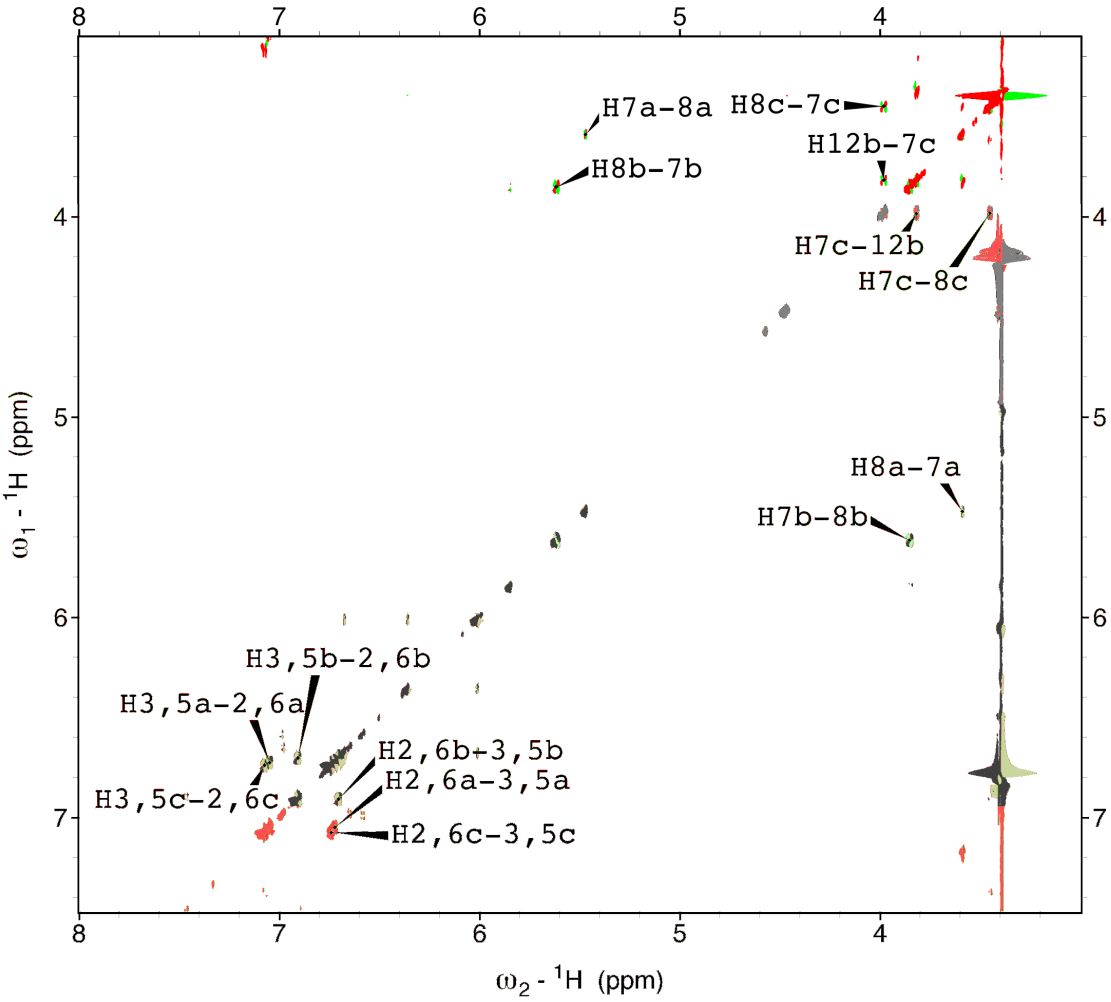

Figure S6. Standard ^{1}H-^{1}H COSY spectrum of vatiparol.

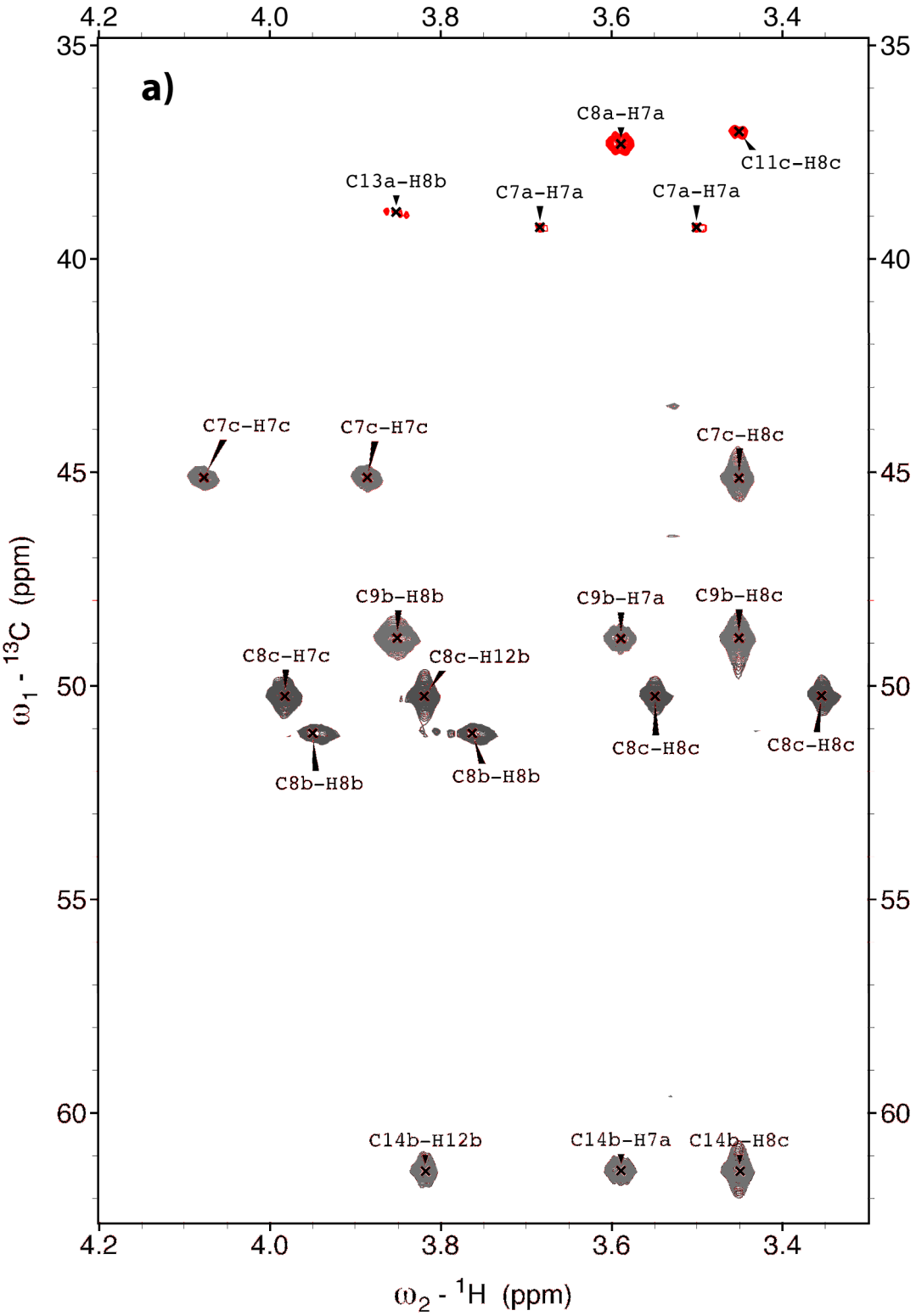
a)
C8a-H7a
C11c-H8c
C13a-H8b
C7a-H7a
C7a-H7a
C7c-H7c
C7c-H7c
C7c-H8c
C9b-H8b
C9b-H7a
C9b-H8c
C8c-H7c
C8c-H12b
C8c-H8c
C8c-H8c
C8b-H8b
C8b-H8b
C14b-H12b
C14b-H7a
C14b-H8c
4.2
4.0
3.8
3.6
3.4
35
40
45
50
55
60
ω1 - 13C (ppm)
ω2 - 1H (ppm)

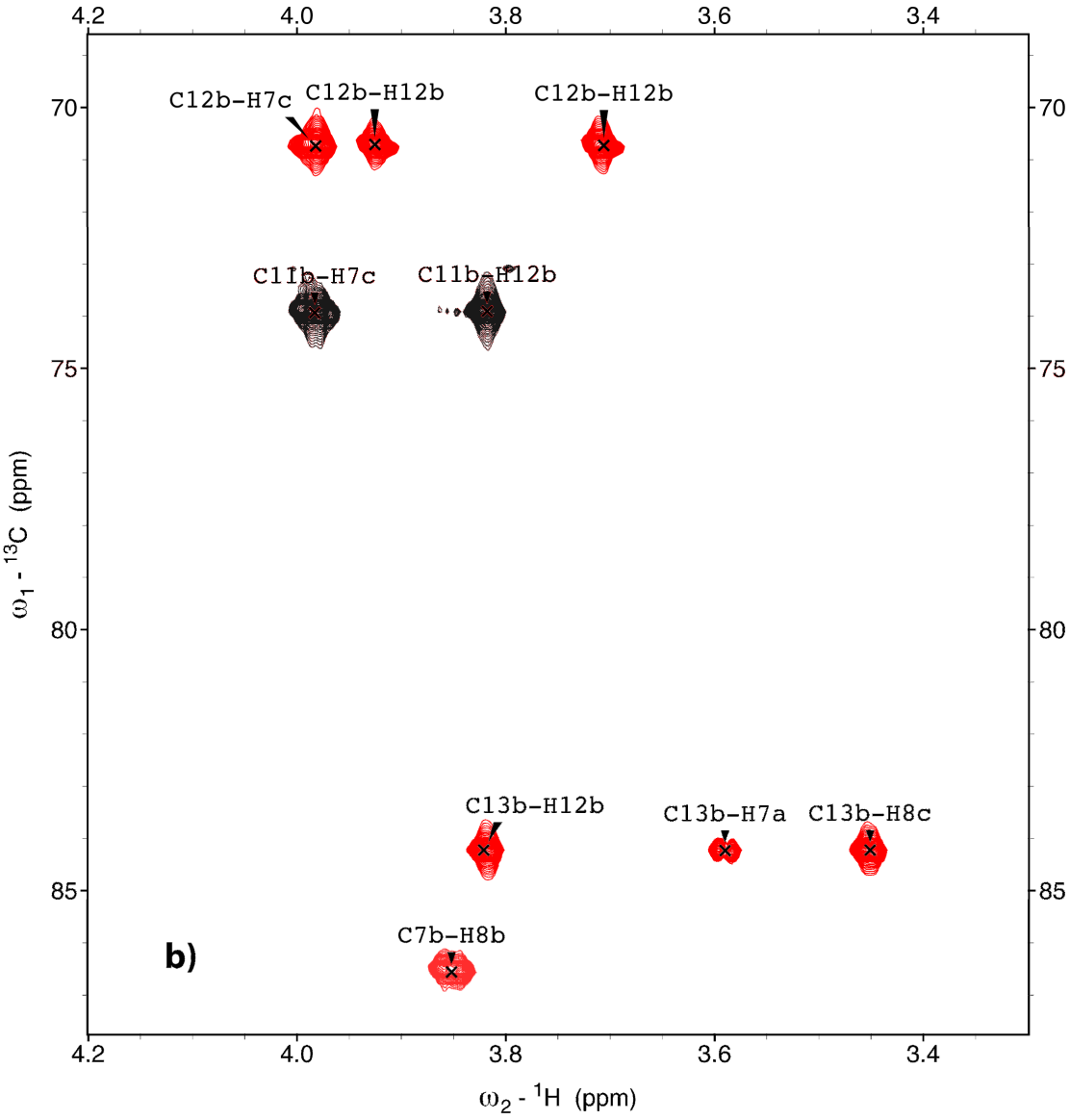
C12b-H7c
C12b-H12b
C12b-H12b
C11b-H7c
C11b-H12b
C13b-H12b
C13b-H7a
C13b-H8c
C7b-H8b
b)
4.2
4.0
3.8
3.6
3.4
70
75
80
85
ω1 - 13C (ppm)
ω2 - 1H (ppm)

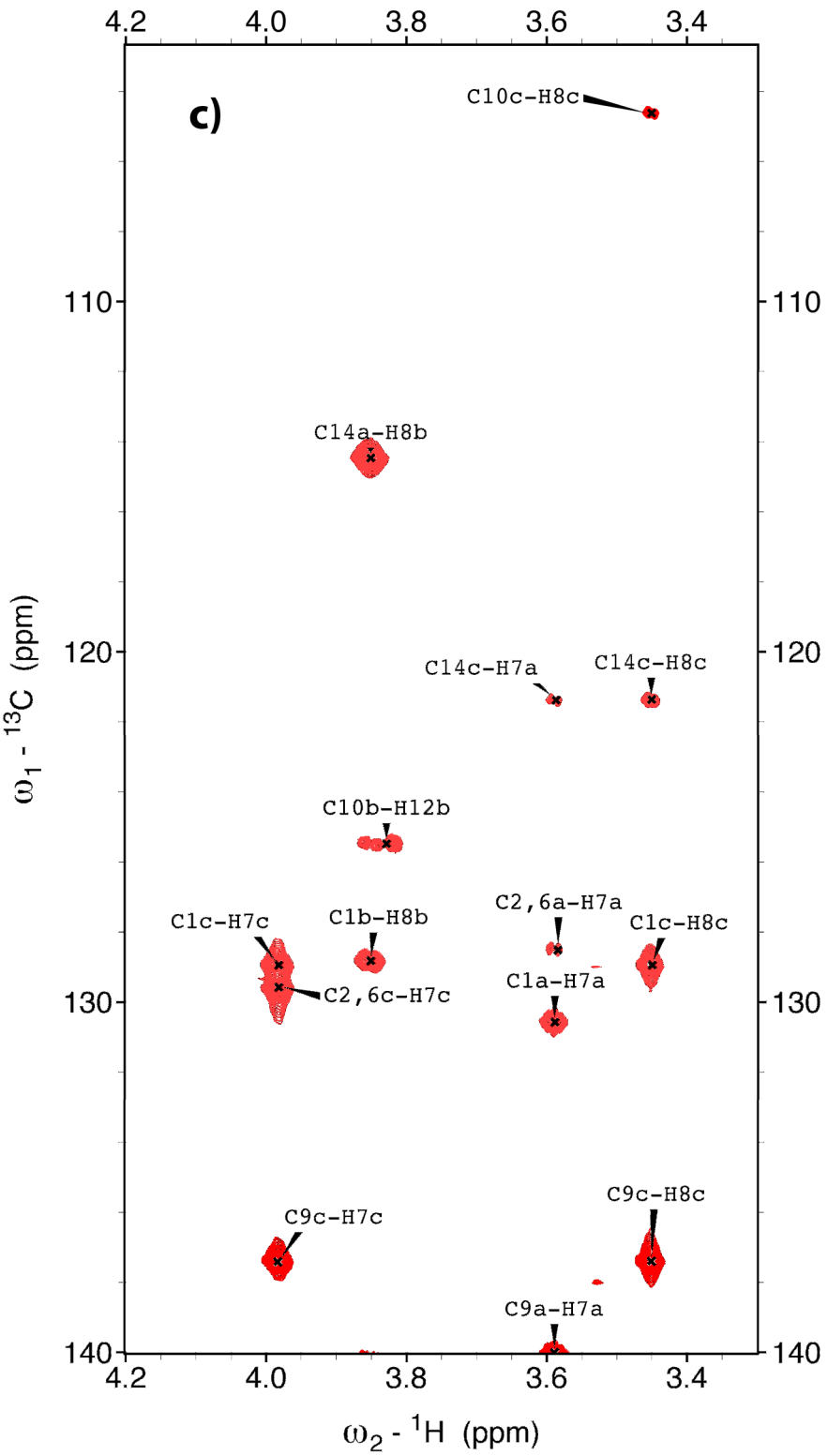
c)
C10c-H8c
C14a-H8b
C14c-H7a
C14c-H8c
C10b-H12b
C1c-H7c
C1b-H8b
C2,6a-H7a
C1c-H8c
C2,6c-H7c
C1a-H7a
C9c-H8c
C9c-H7c
C9a-H7a
4.2
4.0
3.8
3.6
3.4
110
120
130
140
ω1 - 13C (ppm)
ω2 - 1H (ppm)

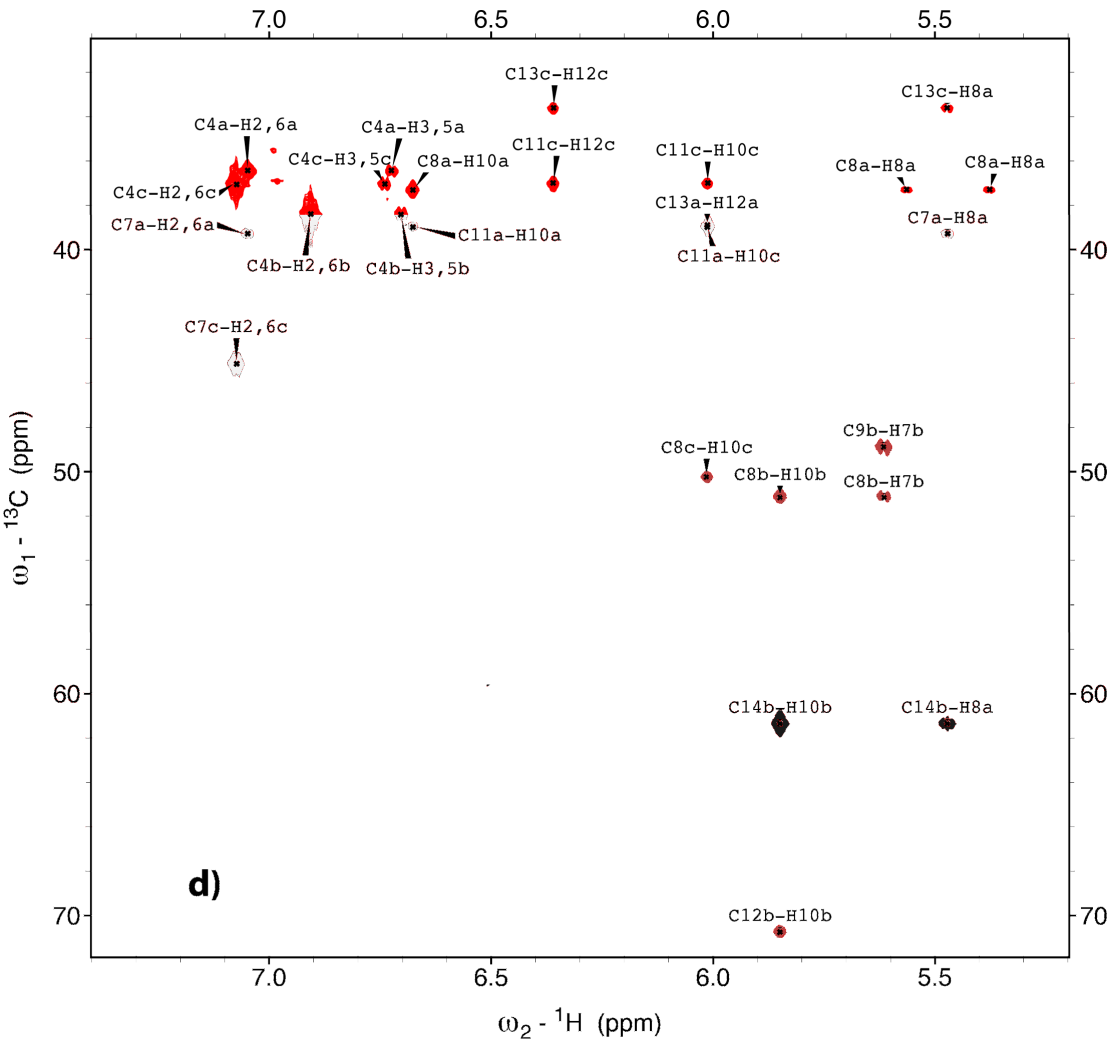
7.0
6.5
6.0
5.5
C13c-H12c
C13c-H8a
C4a-H2,6a
C4a-H3,5a
C11c-H12c
C11c-H10c
C8a-H8a
C8a-H8a
C4c-H3,5c
C8a-H10a
C4c-H2,6c
C13a-H12a
C7a-H8a
C7a-H2,6a
C11a-H10a
C11a-H10c
C4b-H2,6b
C4b-H3,5b
C7c-H2,6c
C9b-H7b
C8c-H10c
C8b-H10b
C8b-H7b
C14b-H10b
C14b-H8a
d)
C12b-H10b
40
50
60
70
ω1 - 13C (ppm)
ω2 - 1H (ppm)

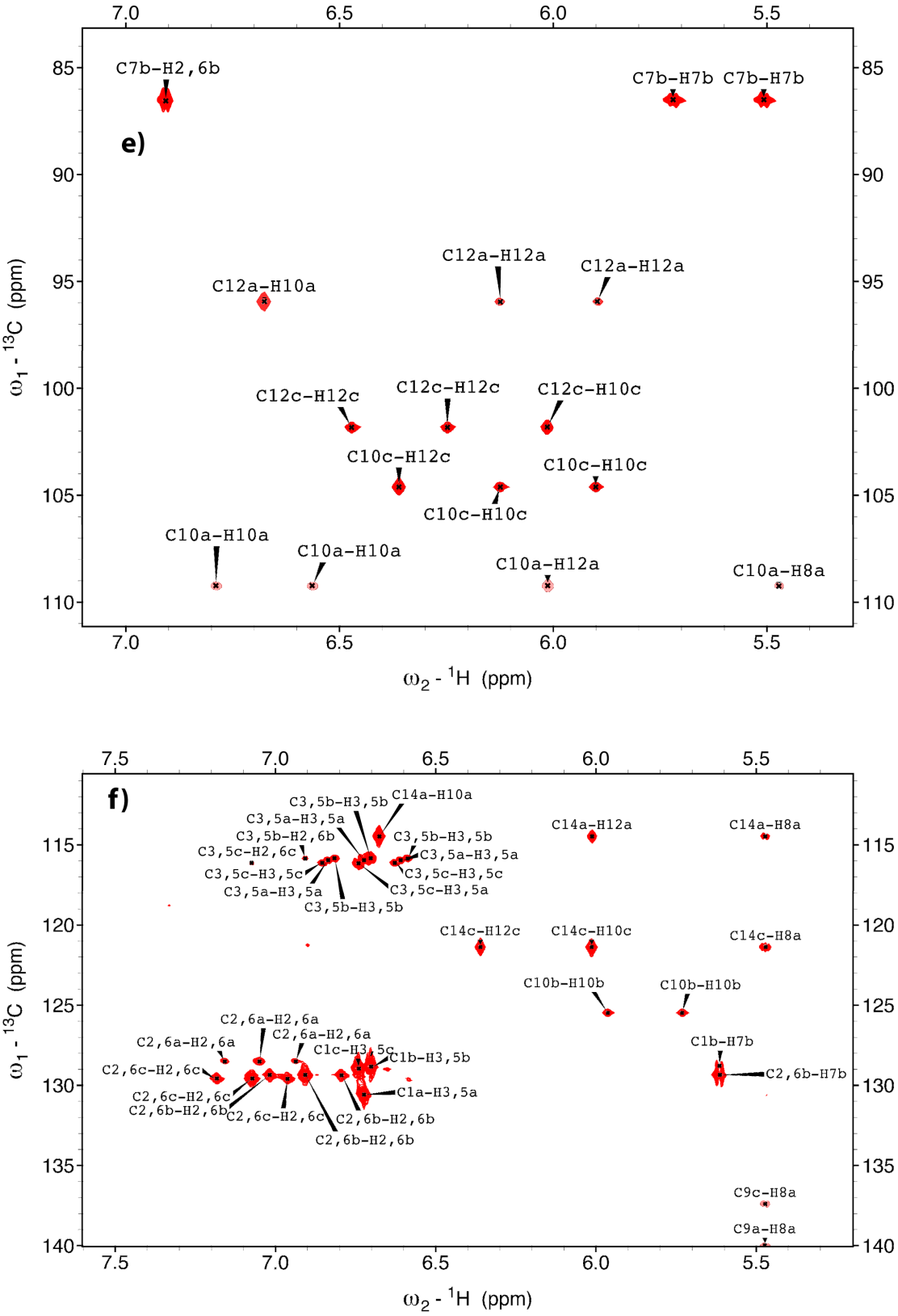

Figure S7. Six expansions of the standard $^{1}H,^{13}C$-HMBC spectrum of vatiparol. a) 3.3-4.2 ppm (^{1}H) and 35-63 ppm (^{13}C), b) 3.3-4.2 ppm (^{1}H) and 71-88 ppm (^{13}C), c) 3.3-4.2 ppm (^{1}H) and 103-140 ppm (^{13}C), d) 5.2-7.4 ppm (^{1}H) and 30-72 ppm (^{13}C), e) 5.3-7.1 ppm (^{1}H) and 83-111 ppm (^{13}C), and f) 5.2-7.6 ppm (^{1}H) and 110-140 ppm (^{13}C).

Table S1. The assignment of ^{1}H and ^{13}C NMR signals of vatiparol acquired in DMSO-d_6.

Proton	Chemical shift [ppm]	Carbon	Chemical shift [ppm]
		C1a	130.6
H2a,6a	7.049	C2a,6a	128.5
H3a,5a	6.723	C3a,5a	115.8
		C4a	156.4
H7a	3.589	C7a	39.3
H8a	5.472	C8a	37.3
		C9a	140.0
H10a	6.676	C10a	109.1
		C11a	158.9
H12a	6.012	C12a	95.8
		C13a	158.9
		C14a	114.5
		C1b	128.8
H2b,6b	6.907	C2b,6b	129.3
H3b,5b	6.705	C3b,5b	115.7
		C4b	158.4
H7b	5.615	C7b	86.4
H8b	3.851	C8b	51.0
		C9b	168.9
H10b	5.849	C10b	125.5
		C11b	193.9
H12b	3.819	C12b	70.7
		C13b	204.2
		C14b	61.4
		C1c	128.9
H2c,6c	7.073	C2c,6c	129.6
H3c,5c	6.74	C3c,5c	116.1
		C4c	157.0
H7c	3.982	C7c	45.1
H8c	3.451	C8c	50.2
		C9c	137.4
H10c	6.013	C10c	104.6
		C11c	157.0
H12c	6.36	C12c	101.8
		C13c	153.6
		C14c	121.4

J-coupling analysis

$^{3}J_{HH}$ couplings were extracted from 1D-^{1}H spectrum, and long-range proton carbon couplings were derived with [^{1}H-^{13}C]-HECADE[6] and [^{1}H-^{13}C]-HSQMBC[7] experiments (Table S2). *J*-coupling analysis shown in Figure S enables to establish the relative configuration of C7a and C8a to be *RS* or *SR*. The configuration of C7b and C8b

was determined as *RR* or *SS* due to the large coupling constant of H7b/H8b and a relative small NOE between the two proton pairs.

Table S2. Long-range proton-proton and proton-carbon coupling constants.

Atoms	$^3J_{HH}$ [Hz]	Atoms	$^3J_{CH}$ [Hz]
H7a-H8a	4.0	H7a-C9a	8.2
H7b-H8b	10.3	H7a-C14c	3.0
H7c-H8c	7.5	H8a-C1a	2.8
H7c-H12b	7.5	H8a-C14b	8.0
		H8b-C7b	-5.6
		H8b-C10b	3.1
		H12b-C10b	2.5
		H7c-C12b	-5.0
		H8c-C10c	1.48

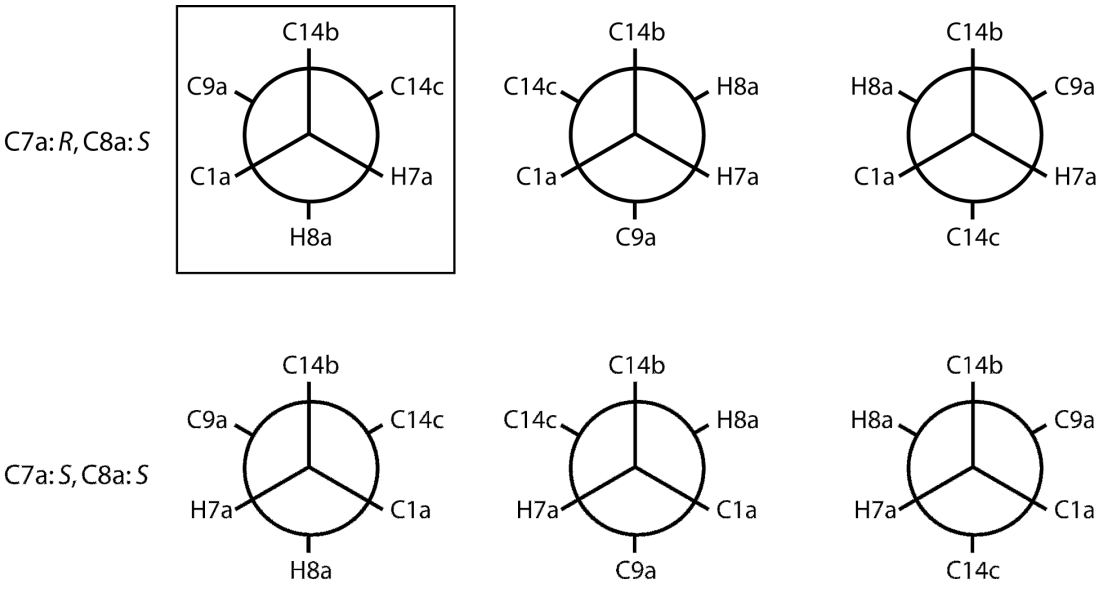

^3J(H7a-H8a)	4.0 Hz	extracted from 1D-^{1}H
^3J(H7a-C9a)	8.2 Hz	extracted from [^{1}H-^{13}C]-HSQMBC
^3J(H7a-C14c)	3.0 Hz	extracted from [^{1}H-^{13}C]-HSQMBC
^3J(H8a-C1a)	2.8 Hz	extracted from [^{1}H-^{13}C]-HSQMBC
^3J(H8a-C14b)	8.0 Hz	extracted from [^{1}H-^{13}C]-HSQMBC

Figure S8. Newman projections for C7a-C8a dihedral derived from *J*-coupling analysis.

Quantitative NOE analysis

Quantitative NOE build-up curves for five different mixing times varying from 200 to 400 ms were derived from NOESY experiments that suppress zero-quantum artefacts. 56 NOEs were integrated at 300 ms mixing time and

translated into proton-proton distances, which were referenced to H10a/H12a, considering the distance between two *meta* proton pairs in a aromatic ring to be 4.29 Å.

Table S3. Proton-proton distances derived from NOESY spectra at 300 ms mixing time.

Proton 1	Proton 2	Distance [Å]	Proton 1	Proton 2	Distance [Å]
H2a,6a	H7a	2.98	H3b,5b	H7b	4.07
H2a,6a	H8a	2.42	H3b,5b	H10b	4.74
H2a,6a	H10a	3.54	H7b	H8b	3.19
H2a,6a	H2,6b	4.23	H7b	H10b	2.50
H2a,6a	H8b	3.21	H7b	H2c,6c	3.46
H2a,6a	H10b	4.84	H7b	H3c,5c	4.95
H3a,5a	H7a	4.29	H7b	H8c	3.74
H3a,5a	H8a	3.75	H8b	H10b	3.56
H3a,5a	H8b	3.57	H8b	H8c	4.21
H3a,5a	H12c	5.32	H10b	H12b	4.57
H7a	H8a	2.81	H10b	H2c,6c	3.45
H7a	H10a	4.40	H10b	H3c,5c	4.59
H7a	H8b	4.25	H10b	H8c	3.90
H7a	H12b	5.20	H12b	H2c,6c	3.29
H7a	H7c	4.14	H12b	H3c,5c	4.99
H7a	H8c	4.05	H12b	H7c	2.50
H7a	H12a	5.06	H12b	H8c	3.99
H8a	H10a	2.94	H12b	H10c	3.68
H8a	H8b	4.17	H2c,6c	H7c	2.76
H8a	H8c	4.50	H2c,6c	H8c	2.56
H8a	H12c	4.70	H2c,6c	H10c	3.13
H10a	H12a	4.29	H3c,5c	H7c	3.94
H10a	H8c	4.56	H3c,5c	H8c	3.79
H10a	H12c	4.42	H3c,5c	H10c	4.17
H12a	H7b	4.73	H7c	H8c	3.09
H2b,6b	H7b	2.96	H7c	H10c	2.43
H2b,6b	H8b	2.76	H8c	H10c	3.45
H2b,6b	H10b	3.38	H10c	H12c	3.81

The violation U for the NOE in Å^2 is defined as:

$$U = \begin{cases} (r^{calc} - r_{\min})^2, & \text{if } r^{calc} < r_{\min}, \\ 0, & \text{if } r_{\min} \le r^{calc} \le r_{\max}, \\ (r^{calc} - r_{\max})^2, & \text{if } r^{calc} > r_{\max}, \end{cases} \qquad \text{(Eq. S2)}$$

where r^{calc} is the back-calculated NOE distance, $r_{\min} = r^{\exp} - 0.4\,\text{Å}$, $r_{\max} = r^{\exp} + 0.4$.

Table S4. The NOE violation (*U*) of configuration *SRSSRSSR* (or its enantiomer *RSRRSRRS)*.

Proton 1	Proton 2	*U* [Å^2]	Proton 1	Proton 2	*U* [Å^2]
H2a,6a	H7a	0.00	H3b,5b	H7b	0.23
H2a,6a	H8a	0.00	H3b,5b	H10b	0.00
H2a,6a	H10a	0.00	H7b	H8b	0.00
H2a,6a	H2,6b	0.00	H7b	H10b	0.04
H2a,6a	H8b	0.01	H7b	H2c,6c	0.00
H2a,6a	H10b	0.00	H7b	H3c,5c	0.00
H3a,5a	H7a	0.01	H7b	H8c	0.00
H3a,5a	H8a	0.11	H8b	H10b	0.00
H3a,5a	H8b	0.00	H8b	H8c	0.00
H3a,5a	H12c	0.00	H10b	H12b	0.00
H7a	H8a	0.00	H10b	H2c,6c	0.00
H7a	H10a	0.00	H10b	H3c,5c	0.00
H7a	H8b	0.00	H10b	H8c	0.00
H7a	H12b	0.05	H12b	H2c,6c	0.00
H7a	H7c	0.00	H12b	H3c,5c	0.00
H7a	H8c	0.00	H12b	H7c	0.00
H7a	H12a	0.00	H12b	H8c	0.00
H8a	H10a	0.00	H12b	H10c	0.18
H8a	H8b	0.00	H2c,6c	H7c	0.00
H8a	H8c	0.00	H2c,6c	H8c	0.00
H8a	H12c	0.00	H2c,6c	H10c	0.00
H10a	H12a	0.00	H3c,5c	H7c	0.08
H10a	H8c	0.00	H3c,5c	H8c	0.06
H10a	H12c	0.00	H3c,5c	H10c	0.00
H12a	H7b	0.00	H7c	H8c	0.00
H2b,6b	H7b	0.00	H7c	H10c	0.00
H2b,6b	H8b	0.00	H8c	H10c	0.00
H2b,6b	H10b	0.08	H10c	H12c	0.00

RDC data and analysis

Table S5. Residual dipolar couplings of vatiparol in PH-gel/DMSO.

CH-vector	$^1D_{CH}$ [Hz]	CH-vector	$^1D_{CH}$ [Hz]
C2a,6a-H2a,6a	-3.7	C10b-H10b	39.6
C7a-H7a	17.5	C12b-H12b	-13.8
C8a-H8a	-4.2	C2c,6c-H2c,6c	-2.01
C10a-H10a	50.3	C3c,5c-H3c,5c	-4.36
C12a-H12a	4.5	C7c-H7c	20.09

C2b,6b-H2,6b	-3.4	C8c-H8c	5.79
C7b-H7b	-44.1	C10c-H10c	-30.59
C8b-H8b	-40.9	C12c-H12c	51.53

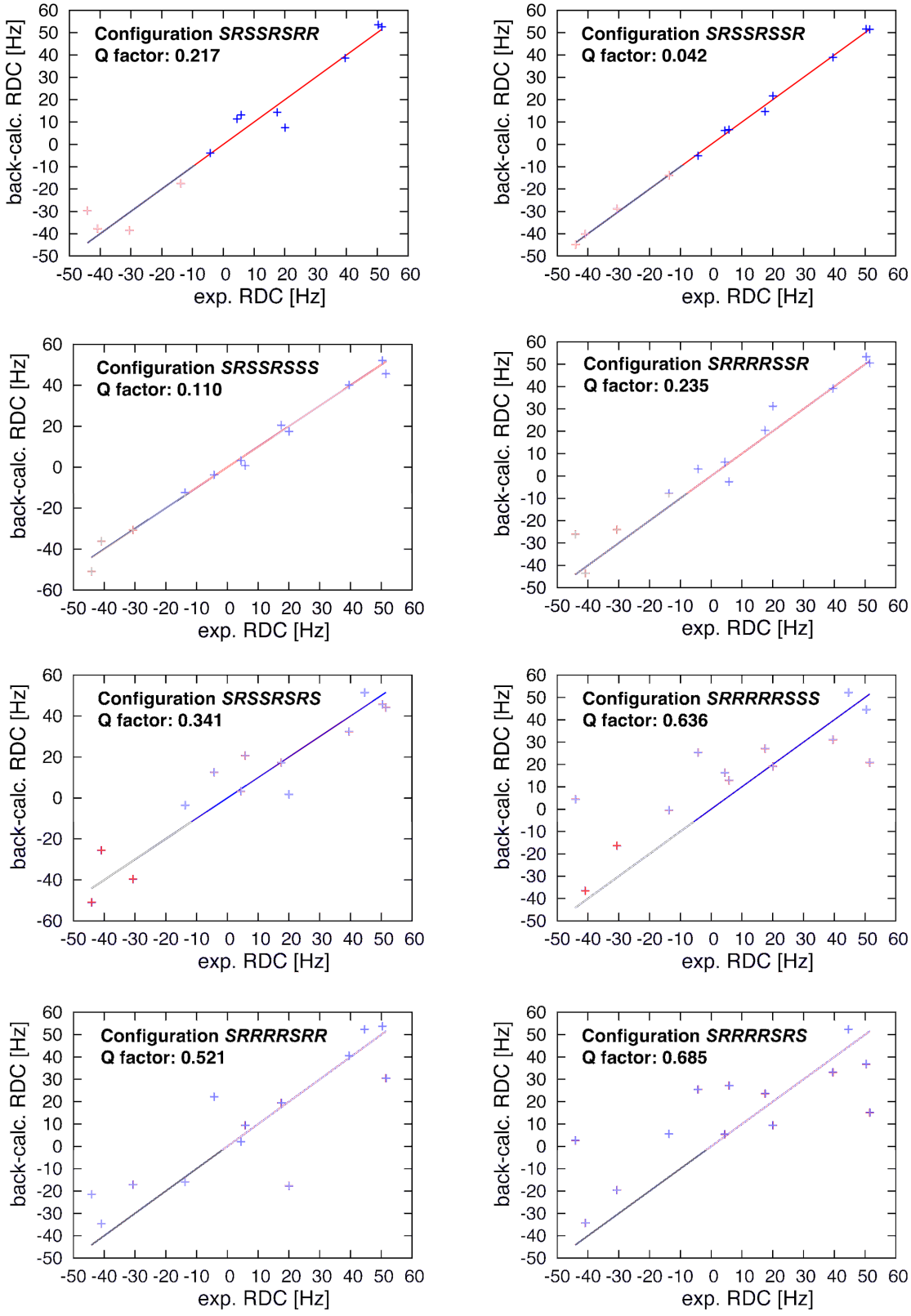

Figure S9. Correlation between experimental and back-calculated RDCs for 8 possible diastereomers.

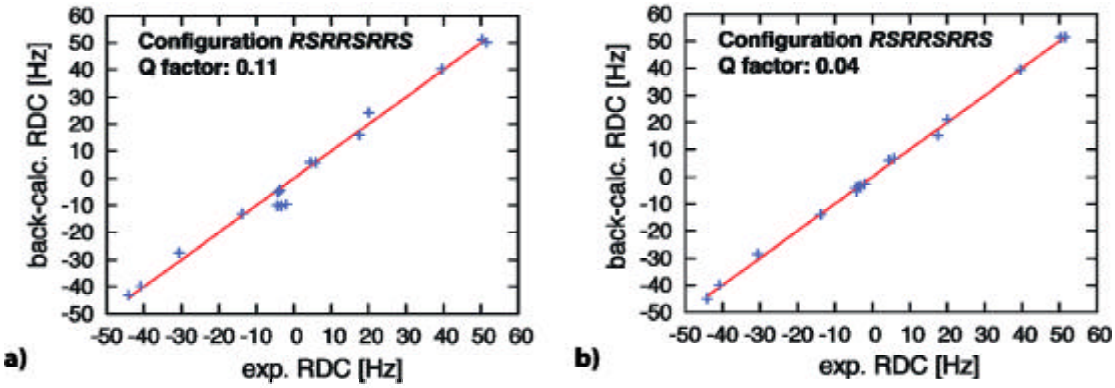

Figure S10. Correlation between experimental and back-calculated RDCs using a) only one orientation of the flexible aromatic ring systems, b) four different orientations of the flexible aromatic ring systems (ring **b** and **c**) found by the conformational search based on molecular mechanics calculations.

Determination of the absolute configuration using chiroptical methods.

Table S6. Experimental and calculated ORD values at different wavelengths.

	$[a]^{exp}$	$[a]^{DFT}$ (configuration: ***SRSSRSRR***)			
l [nm] (source)	**exp.**	**Conformer 1**	**Conformer 2**	**Conformer 3**	**Conformer 4**
589 (Na)	248.04	392.78	350.46	255.44	235.56
578 (Hg)	260.60	410.26	365.93	268.61	247.68
546 (Hg)	302.98	460.62	410.31	308.13	284.06
436 (Hg)	631.08	683.00	593.46	570.17	526.30

Determination of the electric, enthalpy, and Gibbs free energy changes among the reactions between resveratrol-derived radical tautomers A-F

Computational details. The geometric structures of all the resveratrol-derived radical tautomers and the complexes between them were optimized within the density functional theory (DFT) at B3LYP/6–31+G(d,p) level. The vibrational analysis was performed at the same level to show that they had no imaginary frequencies and were all minima in the potential energy surfaces (PES's). To calculate the thermodynamic properties in the solvent environment (water), a polarizable continuum model (PCM) was used. All the calculations in this article were performed using the Gaussian 09 program.

Table S7. The electric, enthalpy, and Gibbs free energy changes among the reactions between A, B, C, D, E and F at B3LYP/6-31+G(d,p).[a]

	Gas-phase			Water solvent		
	?E	*?H*	*?G*	*?E*	*?H*	*?G*
A + C ? AC	19.26	19.30	32.03	31.94	30.67	50.01
A + D ? AD	-10.97	-10.96	2.61	-17.49	-18.88	1.20
A + E ? AE	-8.30	-8.30	-5.39	-0.50	-2.67	19.26
A + F ? AF	-19.12	-19.25	-5.25	-23.79	-25.05	-5.53
B + C ? BC	-19.83	-20.02	-5.73	-22.85	-24.71	-2.94
B + D ? BD	28.52	27.67	44.55	22.58	21.34	40.84
B + E ? BE	0.83	0.66	15.24	-6.14	-7.93	14.09
B + F ? BF	-20.47	-21.09	-5.98	-29.07	-31.46	-8.05

[a.] All the interaction energies were corrected by zero-point energies (ZPE).

Bioactivity results

Vatiparol has low cellular toxicity at 10 µM in vitro.

The cytotoxic effect of vatiparol was assessed in terms of the cell survival using RAW264.7 murine macrophage. The results showed that treatment with vatiparol at 10 µM did not cause RAW264.7 cell death.

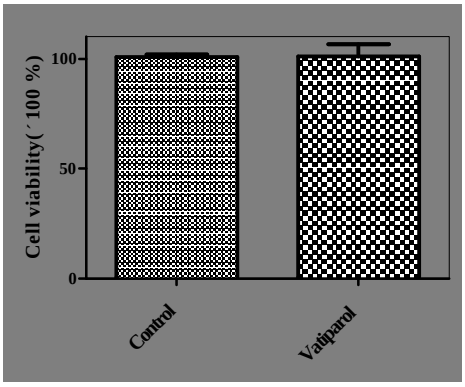

Figure S11. The effect of vatiparol on RAW264.7 cell viability. RAW264.7 cells were treated with vatiparol at 10 µM for 24 h. Cell viability was determined by CCK-8 assay as described in SI Methods. The result expressed as mean ± S.E.M (n=3) is one of three independent experiments. # P < 0.05, compared with control group.

Vatiparol significantly inhibited the MCP-1 production of LPS-stimulated macrophages without affecting on TNF-a and IL-6.

The effect of LPS on the secretion of TNF-a, IL-6 and MCP-1 in RAW264.7 cells is illustrated in Fig. S12. Upon exposure to LPS, RAW264.7 cells (100 ng/mL, 24 h) significantly increased secretions of these proinflammatory mediators. Vatiparol at 10 µM selectively inhibited the MCP-1 production of the LPS-challenged RAW264.7 cells while resveratrol (25 µM) reported is less active and non-selective in the assay system. The action of vatiparol was also confirmed in peritoneal macrophages from three mice with the TNF-a, IL-6 and MCP-1 secretions measured by ELISA. Fig. S13 and Table S8 also illustrate the same selective inhibitory effect of vatiparol on MCP-1 production.

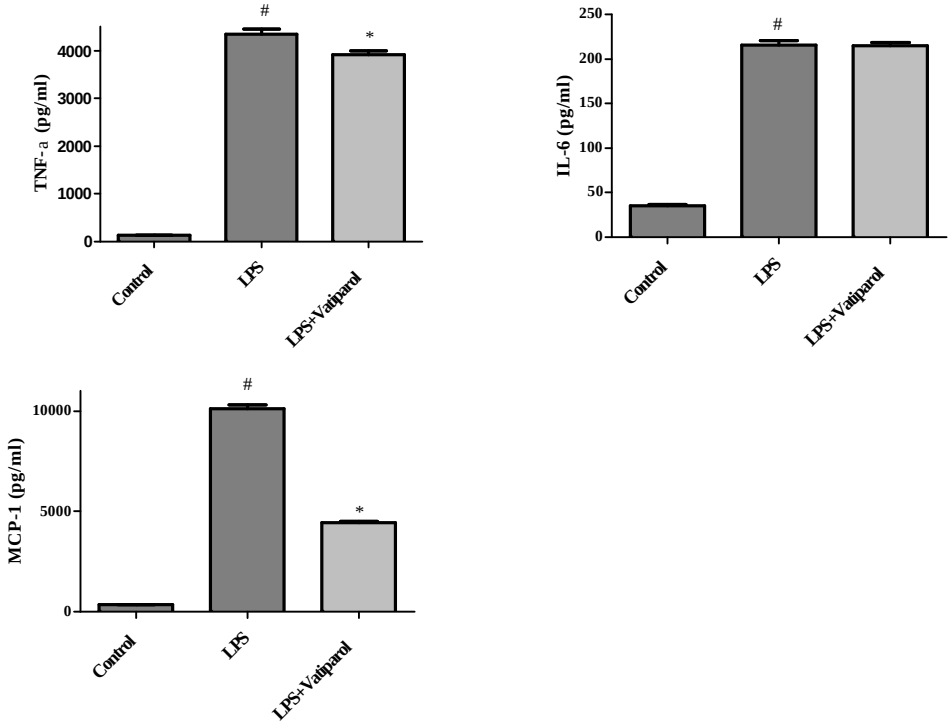

Figure S12. RAW264.7 cells were stimulated with LPS (100 ng/ml) for 24 h in the presence or absence of vatiparol at 10 µM for 2 h, and the levels of TNF-a, IL-6 and MCP-1 in culture supernatants were measured by ELISA. Data presented as mean concentration (pg/ml) ± S.E.M are representative of three independent experiments. # P <0.05, LPS group significantly different from control, * P <0.05, significantly different from LPS group.

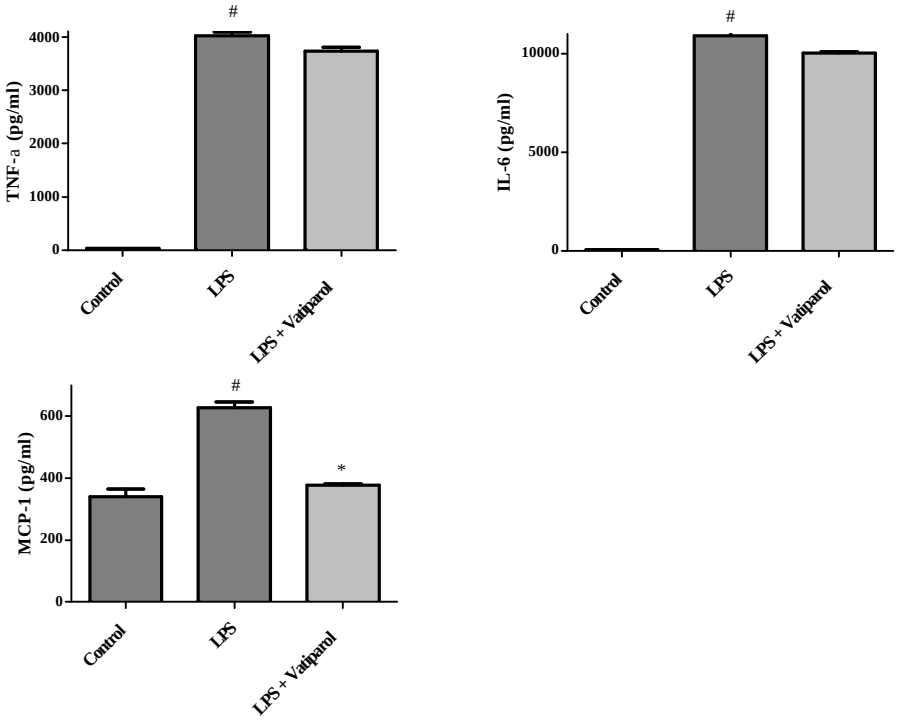

Figure S13. Thioglycolate-elicited peritoneal macrophages were stimulated with LPS (100 ng/ml) for 24 h in the presence or absence of vatiparol at 10 µM for 2 h, and the levels of TNF-a, IL-6 and MCP-1 in culture supernatants were measured by ELISA. Data presented as mean concentration (pg/ml) ± S.E.M are representative of three independent experiments. # P <0.05, LPS group significantly different from control, * P <0.05, significantly different from LPS group.